JOURNAL OF AIRCRAFT
Vol. 32, No. 5, September–October 1995

Experimental and Analytical Investigation of Transonic Limit-Cycle Oscillations of a Flaperon

C. Edward Lan* and Yenpu Chen†
University of Kansas, Lawrence, Kansas 66045
and
Kun-Jan Lin‡
Aero Industry Development Center, Taichung, Taiwan, Republic of China

Forced oscillation testing of a control surface on a rigid model is conducted in a transonic tunnel to identify the possibility of limit-cycle oscillations (LCO) induced by aerodynamic sources. Identification is possible through an energy concept by observing the direction of hysteresis loop in the test data. Two flow devices have also been tested and their effectiveness in eliminating the LCO examined. In addition, test data of hinge moment response in forced oscillation at various frequencies are analyzed through Fourier functional analysis to result in a generalized forcing function in an indicial form. The latter is used in the structural equation of motion for the control surface deflection angle. The resulting nonlinear equation is integrated by Hamming's predictor–corrector method to investigate the effect of structural freeplay. It is demonstrated that if the curves of hinge moment response vs deflection angle in dynamic testing exhibit triple hysteresis, LCO is possible. However, whether the latter actually occurs depends on the initial excitation. Structural freeplay is shown to induce LCO at $M = 0.97$ for the model tested.

Nomenclature

a_{ij} = constants representing lag effect, see Eq. (2)
C = control surface mechanical damping
C_{ave} = average value in the indicial formulation
C_h = hinge moment coefficient, positive to rotate the trailing edge down, based on $\bar{c}$ and S
C_j = reference values, see Eq. (2)
$\bar{c}$ = mean control surface chord, 6.985 cm, or 2.75 in.
E_{ij} = constants associated with the zero-lag response, see Eq. (2)
I = control surface polar moment of inertia
k = reduced frequency, $\omega l/V$
k_δ = control surface hinge stiffness constant
l = reference length, $\bar{c}$
M = freestream Mach number
m = number of Fourier terms
q = freestream dynamic pressure
S = control surface reference area, 208.39 cm^2, or 32.3 in.^{2}
t = time
t' = nondimensional time, tV/l
V = freestream velocity
α = angle of attack
Δt = time step size
δ = variation in angle of deflection, $\delta_0 \cos kt'$
δ_m = mean angle of deflection, -0.5 and 2 deg in the test
δ_s = region of structural freeplay
δ_t = total angle of deflection, $\delta_m + \delta$
δ_0 = amplitude of angle-of-deflection variation
θ = kt'
τ = dummy time integration variable
ϕ = phase angle

Received Aug. 30, 1994; revision received Feb. 1, 1995; accepted for publication Feb. 2, 1995.

*Bellows Distinguished Professor of Aerospace Engineering and the Center for Excellence in Computer Aided Systems Engineering. Associate Fellow AIAA.
†Graduate Research Assistant.
‡Deputy Chief, Aerodynamics Department.

Introduction

THE history of the control surface buzz problem, or limit-cycle oscillations (LCO), started around 1945, when aileron vibration was first encountered in high-speed subsonic flight.[1] In flight testing of the Lockheed P-80 jet fighter aircraft, a low-amplitude aileron LCO was encountered at a Mach number of 0.87, and proved hazardous at a higher Mach number, resulting in permanent damage to the aileron.[2] As it is understood, transonic LCO phenomena are mainly caused by shock motion involving shock-induced flow separation.[3] An excellent review of these phenomena was presented recently by Cunningham.[3]

Although flight testing will provide accurate LCO characteristics of a configuration, such information is fragmentary and hardly ever systematic. Because LCO occurs within a relatively narrow region in the flight envelope, it may not be detected during flight testing. As a result, many control surface LCO incidents occur. Therefore, a better method of LCO detection is needed.

Virtually all the information about control surface oscillations comes from wind-tunnel and flight measurements. A conventional wind-tunnel investigation involves the fabrication of sophisticated dynamic models, a very costly and time-consuming process. As it was determined in the wind-tunnel testing,[4] LCO of a control surface can be described as a single degree-of-freedom oscillation. This result provides a basis to the present method of testing. The present research combines wind tunnel testing of a rigid model and theoretical aerodynamic modeling to determine a general forcing function. Using this forcing function, the structural equation of motion is integrated numerically to predict control surface LCO. This approach is more cost-effective and time-efficient than testing dynamic models. The present research was initiated to find possible reasons of control surface LCO of a flight test vehicle and to determine an effective way to eliminate it.

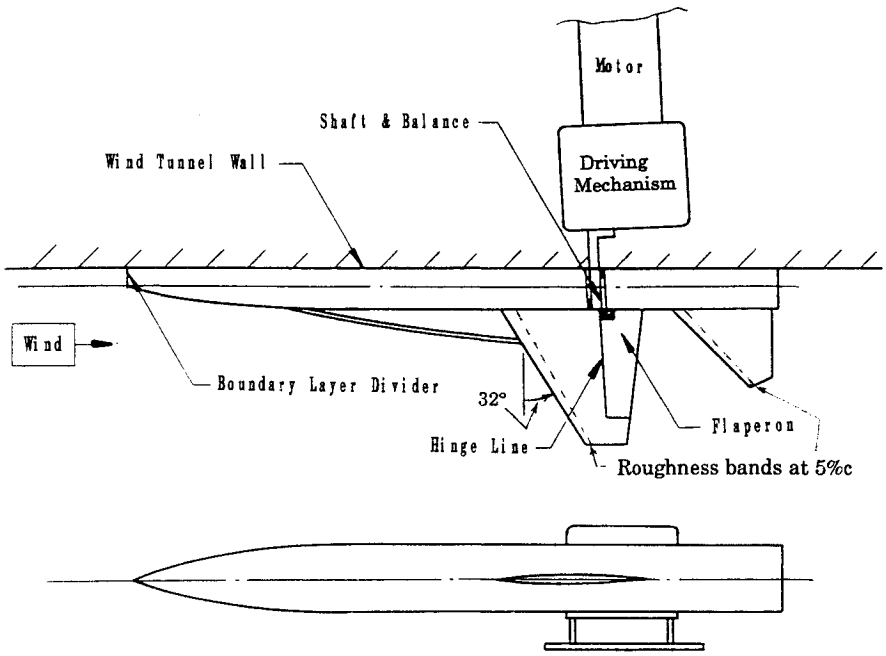

Fig. 1 Test model configuration.

Test Facilities and Models

The test was conducted in the blowdown trisonic wind tunnel at Aero Industry Development Center (AIDC) with a 4 × 4 ft test section and perforated walls. The tunnel Mach number could be varied from 0.3 to 4.0.

Test Model

A rigid half-model was chosen for easy installation of the driving mechanism. The configuration included body, strake (or leading-edge extension), wing, and horizontal tail (Fig. 1) to represent a typical combat aircraft. The wing had a swept-back angle of 32 deg and a span to mean chord ratio of 3:1. The wing had a NACA 64 section of thickness ratio 5%. The ratio of the control surface span to wingspan and the surface area ratio were 0.6 and 0.1, respectively. A bridge of strain gauges was installed on the drive axis of the control surface. The design concept of the driving mechanism was that an electrical servomotor was connected to a driving cam to give harmonic motion to a rotating control shaft. The oscillation amplitude of the control surface was controlled by the size of the cam (Fig. 2).

Test Method and Procedures

The test Mach number varied from 0.9 to 1.05, and the corresponding unit Reynolds number was 7×10^6/ft. Roughness strips were applied at selected locations over the surfaces of forebody, wing, and horizontal tail of the half-model to fix transition of the boundary layer. The angle of attack was 2 deg. Two flaperon mean deflection angles were selected (-0.5 and 2 deg), and the maximum oscillation amplitude for both flaperon deflection angles was 3 deg.

The control surface oscillation was controlled by varying the rpm of the motor to produce different frequencies at different Mach numbers. The hinge moment coefficient C_h and oscillation angle δ were recorded by strain gauges and the angular potentiometer, respectively. The high-frequency strain gauges were mounted on the drive axis of the control surface. The measured signals were filtered to reduce the interference from the 60-Hz noise. The sampling rate of data acquisition for an oscillographic recorder was set to 500 Hz. The acquired data on PDP-11/44 was transmitted to a personal computer for digital signal processing and data analysis.

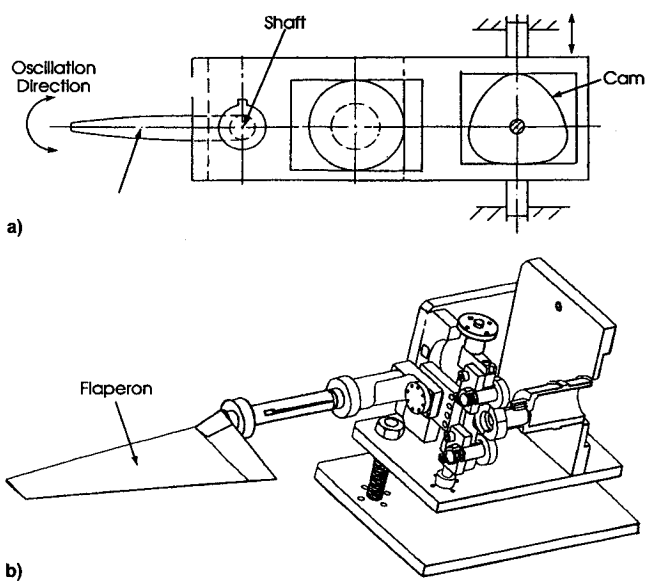

Fig. 2 Driving mechanism of the forced oscillation test rig: a) driving mechanism design concept and b) arrangement of model control surface and driving mechanism.

Method of Analysis

Aerodynamic Modeling

In the present research, we will determine the LCO-producing forcing function (i.e., the hinge moment) separately and solve the structural equation of motion afterwards. Then the same forcing function can be repeatedly used, even when the structural characteristics are changed.

Consider a flap oscillation:

$$\delta(t) = \delta_m + \delta_0 \cos(kt') \tag{1}$$

where δ_m is the mean angle of oscillation, δ_0 is the oscillation amplitude, k is the reduced frequency, and t' is the dimensionless time. Using a suitable set of aerodynamic hinge-moment responses to flap harmonic motions at different frequencies, we can build up a general forcing function mentioned above through Fourier functional analysis.[5,6] The final expres-

sion for the forcing function is in the nonlinear indicial form and is given by

$$C_h(t') = C_{h_{\text{indicial}}}[t' - \tau, \delta(\tau), \dot{\delta}(\tau)]_{\tau=0} + C_{\text{ave}} + \sum_{j=1}^{m} C_j \times (E_{1j}\dot{\delta}_j + E_{2j}\ddot{\delta}_j) + \sum_{j=1}^{m} C_j * \int_0^{t'} \frac{\mathrm{d}(\mathrm{AF})_j}{\mathrm{d}\delta} * [1 - a_{1j}e^{a_{3jj}(t'-\tau)} - a_{2j}e^{a_{4jj}(t'-\tau)}] \frac{\mathrm{d}\delta(\tau)}{\mathrm{d}\partial\tau} d\tau + \frac{l}{V_\infty} \sum_{j=1}^{m} C_j * \int_0^{t'} \frac{\mathrm{d}(\mathrm{AF})_j}{\mathrm{d}\dot{d}} \times [1 - a_{1j}e^{a_{3jj}(t'-\tau)} - a_{2j}e^{a_{4jj}(t'-\tau)}] \frac{\mathrm{d}\dot{\delta}(\tau)}{\mathrm{d}\tau} \quad (2)$$

where AF is the amplitude function and C_{ave} is the average value being a function of δ_m, the mean angle about which the oscillations in the test takes place. It should be noted that δ in Eq. (2) denotes a perturbation from δ_m. The first term in Eq. (2) is the amplitude of C_h, when δ is abruptly changed to $\delta(0)$ at $\tau = 0$ and represents an initial value in the indicial lift formulation.[7]

To perform the time integration in Eq. (2) for arbitrary motions, a trapezoidal rule is chosen because the time step used is very small. Note that for given δ and $\dot{\delta}$ at time t, the time integration in Eq. (2) must be performed by using an equivalent frequency or amplitude and a phase angle because the model coefficients have been obtained in frequency domain. At a given time of an arbitrary motion, the deflection angle and its time rate, δ_1 and $\dot{\delta}_1$, can be described by

$$\delta_1(\tau) = \delta_m + \delta_0 \cos(k\tau + \phi) \quad (3a)$$

$$\dot{\delta}_1(\tau) = -\delta_0 k \sin(k\tau + \phi) \quad (3b)$$

By knowing the harmonic model's mean angle of deflection δ_m and amplitude δ_0, an equivalent frequency k and an equivalent phase angle ϕ at a given instantaneous time τ can be solved directly to give

$$k = \frac{|\dot{\delta}_1|}{\sqrt{\delta_0^2 - (\delta_1 - \delta_m)^2}}$$
$$\phi = \tan^{-1}[(\delta_1 - \delta_m)/(\dot{\delta}_1/k)] - k\tau \quad (4)$$

To smooth out possible discontinuity in response when the given motion has a sudden change in $\dot{\delta}$, a δ_0 that is slightly greater than the actual test amplitude is frequently used. It should be emphasized that this does not change the instantaneous values of δ_1 and $\dot{\delta}_1$ in the actual motion. It merely changes the values of k and ϕ. Applicability of this concept has been demonstrated in Refs. 5 and 6 for rigid model pitching motion.

Numerical Integration

The structural equation of motion is given by

$$I\ddot{\delta} + C\dot{\delta} + k_\delta\delta = q_\infty S\bar{c} \cdot C_h(t') \quad (5)$$

where $\cdot = \mathrm{d}/\mathrm{d}t$, and t is in seconds and needs to be nondimensionalized by V/l before integration, because C_h is a function of t'. In the present application, I and k_δ are obtained from a finite element analysis of the full-scale structure and are given by $I = 3.61$ ft-lb-s^2, $C = 0$, and $k_\delta = 187{,}500$ ft-lb.

The right-hand side (RHS) of Eq. (5) contains highly nonlinear and time-dependent terms in the motion variable δ. To accurately integrate this equation, Hamming's predictor–corrector method[8] is chosen. To start the integration, a fourth-order Runge–Kutta technique is used to obtain the solutions at three time steps before the predictor–corrector procedure starts, providing that the initial conditions $\delta(0)$ and $\dot{\delta}(0)$ are given.

Results and Discussion

Wind-tunnel forced oscillation tests were conducted on a fighter configuration with a large-span flaperon (Fig. 1) at transonic speeds, and the hinge moments were measured corresponding to the instantaneous flaperon deflection angle. Here, only data at $M = 0.97$, $\alpha = 2$ deg, and $\delta_m = -0.5$ deg are presented and analyzed.

Data Reduction and Test Results

Tests were conducted under static condition ($k = 0$), wind-off and wind-on forced oscillation at two flaperon mean angles of deflection, and five reduced frequencies. Raw wind-on oscillation test data contain 500 points over a number of cycles. These data are first separated into a number of cycles of oscillation. Then their amplitudes are adjusted slightly to attain a constant angle of maximum deflection. Finally, the ensemble-averaging over cycles is made to result in one complete set of data in one cycle. The wind-off data are then

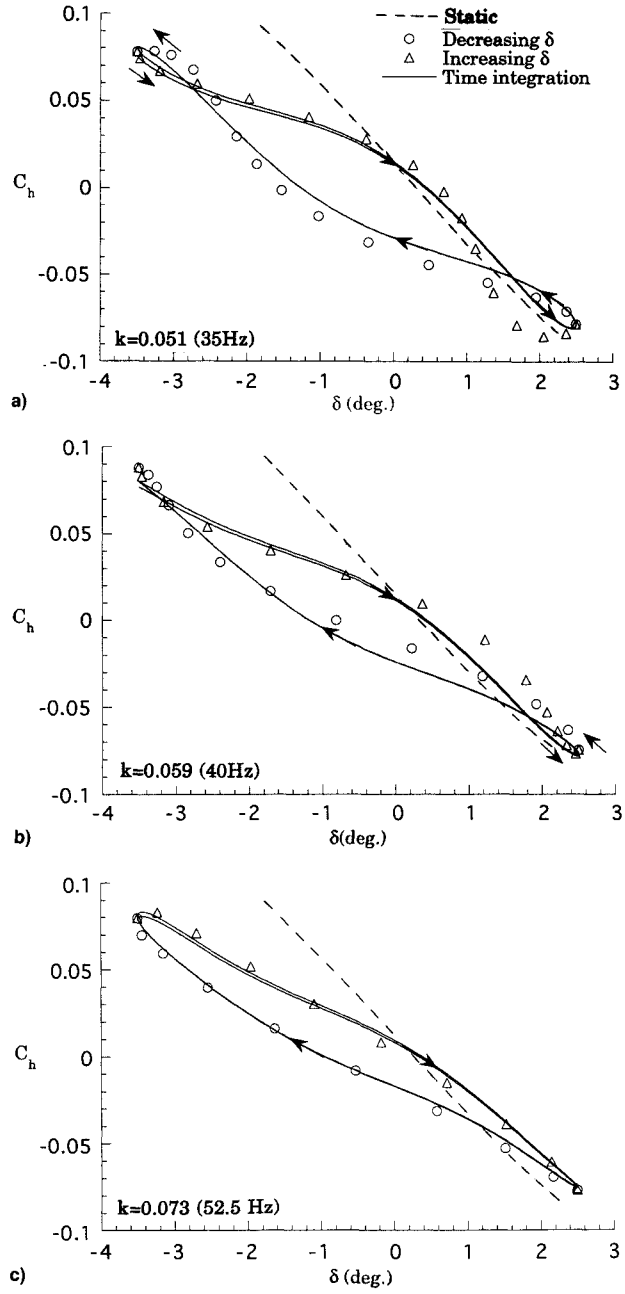

Fig. 3 Wind-tunnel test data and results of indicial integration for a control surface oscillation at $M = 0.97$, $\alpha = 2$ deg, and $\delta_m = -0.5$ deg.

subtracted to provide the final dynamic hinge moment coefficient C_h.

Results at $M = 0.97$ and $\delta_m = -0.5$ deg at three reduced frequencies are presented in Fig. 3. Modeling results based on the indicial formulation are also shown. Data are also taken at two lower frequencies (20 and 25 Hz, not shown). But the results do not show significant hysteresis as compared with those at higher frequencies shown in Fig. 3. Because of the sudden change in the hysteresis loop between 25–35 Hz, it requires too many Fourier terms to provide a good model. Since it is known from a dynamic model testing that limit-cycle oscillation exists at higher frequencies, only the last three sets of data at higher frequencies are used in the modeling.

As shown in Fig. 3, there are triple hysteresis loops in the hinge moment response for $k = 0.051$ and 0.059. The direction of the loop can be used to explain instability by using the following energy integral with only the first harmonics in the hinge moment response:

$$\text{work} = \oint c_h \, d\delta = \oint [c_{h_r} \cos(kt') - c_{h_i} \sin(kt')] \, d(\delta_0 \cos kt') = \pi c_{h_i} \delta_0 \tag{6}$$

The work input is positive if $c_{h_i} > 0$, and hence, the system is unstable. If $c_{h_i} > 0$, the hysteresis loop is clockwise. Therefore, at higher frequencies the flaperon motion is unstable around δ_m; but it becomes stable at higher values of δ and frequency (cf. curve in Fig. 3 for $k = 0.073$). This is a general characteristic of limit-cycle oscillations.

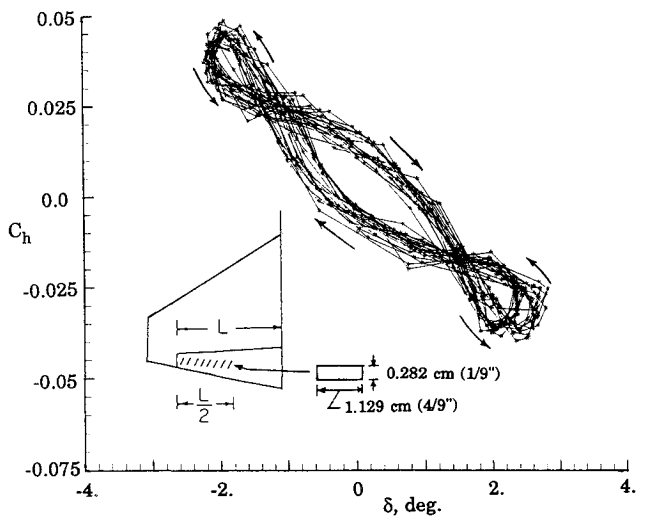

Fig. 4 Test results with vortex generators on the control surface at $M = 0.97$, $\alpha = 2$ deg, and $\delta_m = -0.5$ deg, and frequency of 40 Hz.

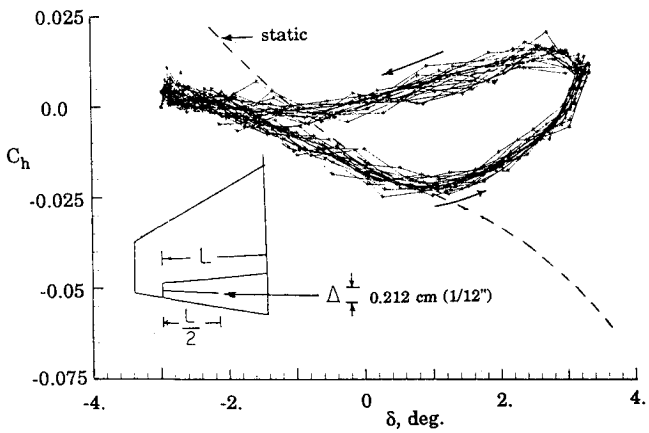

Fig. 5 Test results with spoilers on the control surface at $M = 0.97$, $\alpha = 2$ deg, and $\delta_m = -0.5$ deg, and frequency of 40 Hz.

In Fig. 3, it is also shown that the static control effectiveness (i.e., the slope of the $C_h - \delta$ curves) is generally higher than the equivalent or average dynamic values. This is consistent with the test results of Ref. 9, where the equivalent dynamic C_h was defined as the resultant of the in- and out-phase components of the first harmonic plus the in-phase component of the second harmonic.

Various flow control devices have also been tested to determine if they are effective in eliminating the clockwise hysteresis loop. Typical sets of results with vortex generators and spoilers of triangular cross section (both located at the mid-flaperon chord) are presented in Figs. 4 and 5, respectively, for $k = 0.059$. Figure 4 shows that the vortex generators are ineffective; whereas Fig. 5 shows that the spoilers eliminate the LCO at the expense of slightly reducing the static control effectiveness (cf. the static curves in Figs. 3 and 5). More detailed measurements (including the static hinge moments) with the vortex generators were not conducted as soon as the vortex generators were found to be ineffective in controlling the LCO. The present test technique was also used to optimize the location and size of the spoilers. Using spoilers to reduce or eliminate the LCO on a vertical tail have been investigated in the past.[10,11] Their effectiveness for the present configuration have also been verified in flight testing.

Effect of Structural Freeplay by Analysis

The equation of motion [Eq. (5)] can be integrated to determine the necessary mechanical damping C to eliminate the LCO at given flight conditions. However, the effect of structural freeplay will be illustrated here instead.

A plot of typical load-deflection relation obtained by simple static tests conducted on a wing-flap combination is presented in Fig. 6. Freeplay is defined by extending the best straight lines through zero load. System stiffness may then be obtained from the slopes of the curves away from the zero point. In addition to this flat spot type of freeplay, there are two other types of freeplay effects, namely hysteresis type and cubic type.[12] In the present model, only the flat type of freeplay is considered. The structural stiffness constant k_δ in Eq. (5) is replaced by a piecewise linear function $k_\delta(\delta)$. The piecewise linear function $k_\delta(\delta)$ is given by

$$k_\delta(\delta) = \begin{cases} k_s, & \delta > \delta_s \\ 0, & -\delta_s < \delta < \delta_s \\ k_s, & \delta < -\delta_s \end{cases} \tag{7}$$

In integrating the equation of motion [Eq. (5)], initial conditions are needed. Figure 7 presents the ensuing flaperon motion without structural freeplay after it is disturbed with two sets of initial conditions at $M = 0.97$. Both sets of initial conditions show oscillations converged smoothly to reach approximately -0.5-deg offsets, where the model mean angle of deflection lies. Oscillation with a larger initial velocity causes the oscillation to be more symmetric about its final offset δ value. Referring to Fig. 3, we expect that the oscillations should diverge within the indicated range of motion. This apparent inconsistency can be explained by the fact that the flap motion not only produces damping or undamping, but also generates aerodynamic stiffness, which increases the system frequency. At a higher frequency, the motion may become stable again (Fig. 3c). For a nonlinear system to enter an unstable motion, it must be positioned in the unstable region on the phase plane. One way to change the system frequency, and hence, the position in the phase plane, is to introduce structural freeplay. Realistically, zero freeplay is an ideal condition. It is therefore imperative to simulate flaperon oscillations in a nonzero freeplay environment.

As depicted in Fig. 8, flaperon LCO is predicted when a structural freeplay of 1 deg is assumed. It can be clearly seen from Figs. 8a and 8b that a hinge moment coefficient of about -0.01 corresponding to a 0 deg of initial δ builds up the LCO-

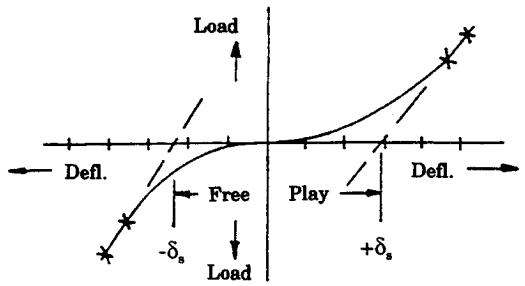

Fig. 6 Definition of structural freeplay.

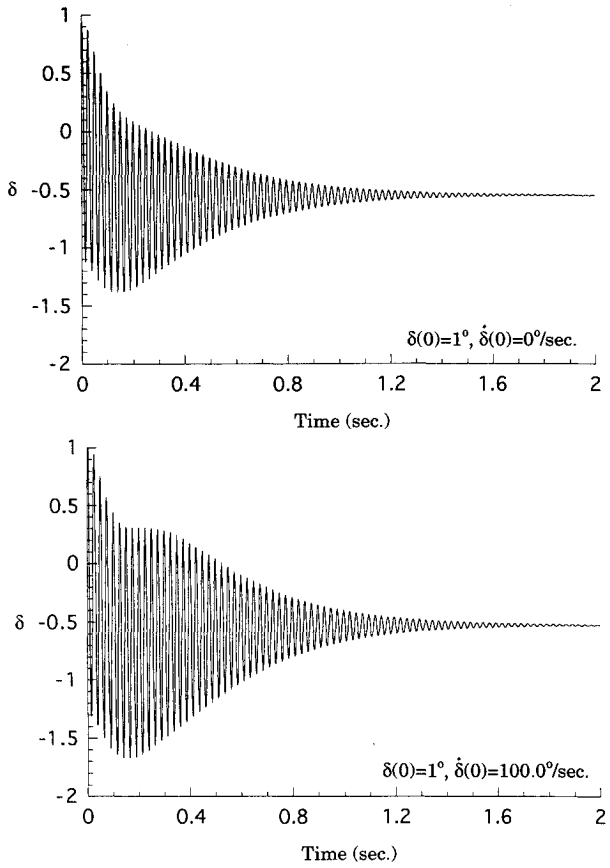

Fig. 7 Time history of flaperon oscillation at $M = 0.97$, $\alpha = 2$ deg, and $h = 5000$ ft.

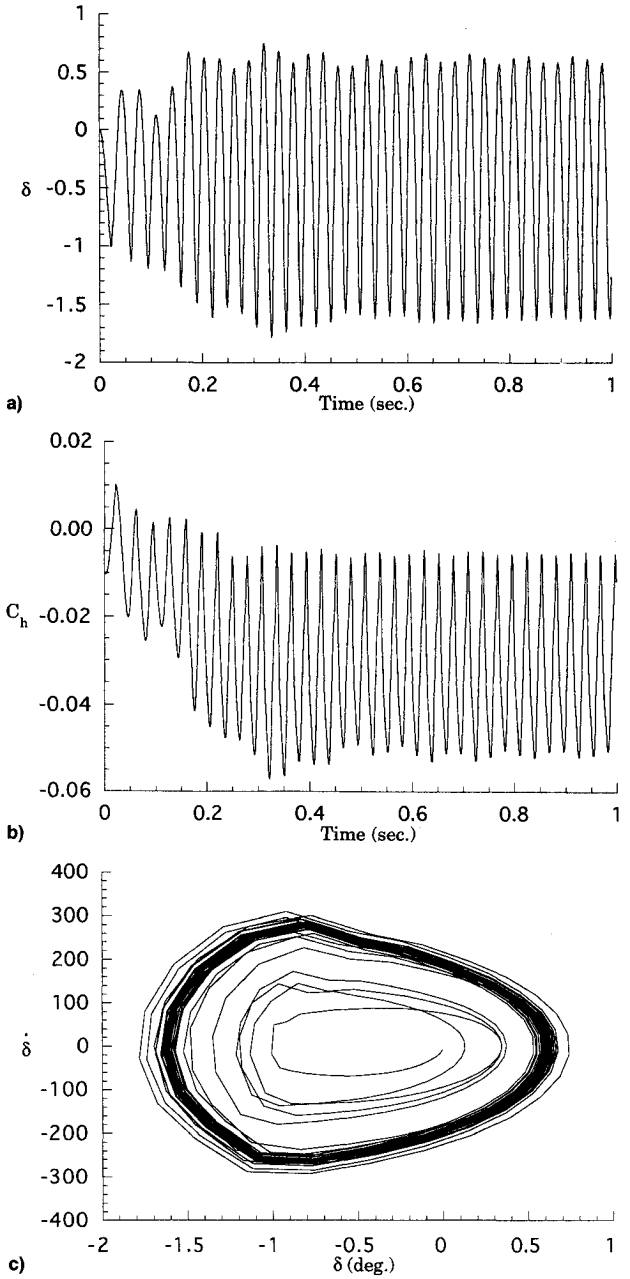

Fig. 8 Time history of flaperon oscillation at $M = 0.97$, $\alpha = 2$ deg, and $h = 5000$ ft. $\delta(0) = 0$ deg, $\dot{\delta}(0) = 0$ deg/s, $\delta_s = 1$ deg: a) variation of flaperon deflection, b) variation of hinge moment, and c) phase plane diagram.

starting conditions, which is reasonable as the angle of attack is +2 deg to provide a tendency of upward motions. From the time history, it is apparent that higher frequency terms are present in the solution, but gradually decay as the limit cycle is established around $t = 0.35$ s. The reduced frequency of LCO is approximately equal to a constant value of 0.067 (34.78 Hz), well within the frequency range covered by the present model (from $k = 0.051$ at 35 Hz to $k = 0.073$ at 52.5 Hz) at $M = 0.97$. The LCO occurs with respect to a mean angle of roughly −0.5 deg, with the amplitude staying around 1.1 deg throughout the time simulated. On the phase plane (Fig. 8c), stable limit cycles are represented by closed curves. Figure 9 depicts the results obtained at higher initial deflections with an initial velocity. The oscillation diverges in a few cycles after started. This set of initial conditions, being outside the closed curves on the phase plane, induces unstable motion and a limit-cycle oscillation cannot be attained.

Figure 10 presents LCO under the same initial conditions as in Fig. 8, except the structural freeplay was set at 0.5 deg. The results show a much smaller amplitude of oscillation, which is not constant and chaotic to some extent. The oscillation takes place roughly about the model mean angle of

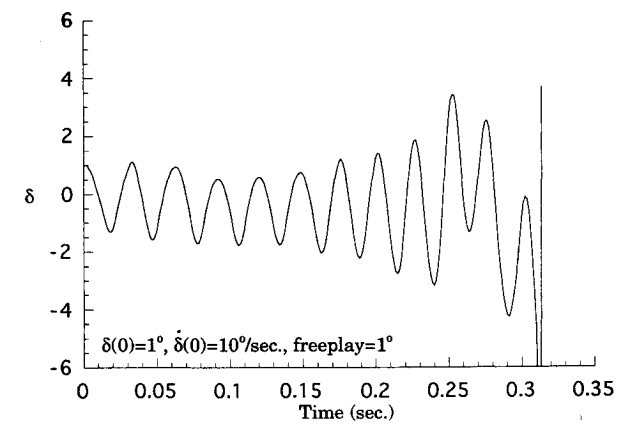

Fig. 9 Time history of flaperon oscillation at $M = 0.97$, $\alpha = 2$ deg, and $h = 5000$ ft.

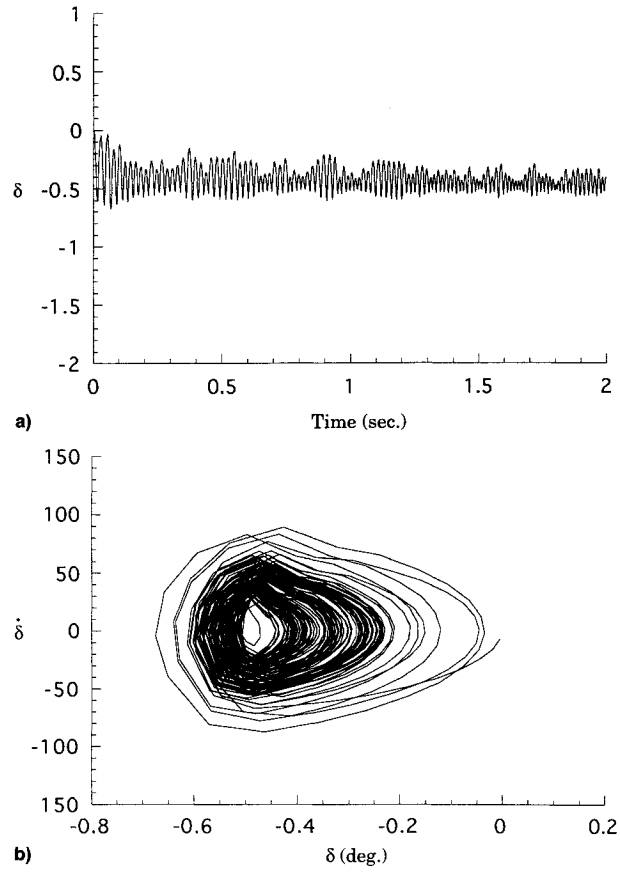

Fig. 10 Flaperon LCO at $M = 0.97$ and $h = 5000$ ft. $\delta(0) = 0$ deg, $\dot{\delta}(0) = 0$ deg/s, $\delta_s = 0.5$ deg: a) variation of flaperon deflection and b) phase plane diagram.

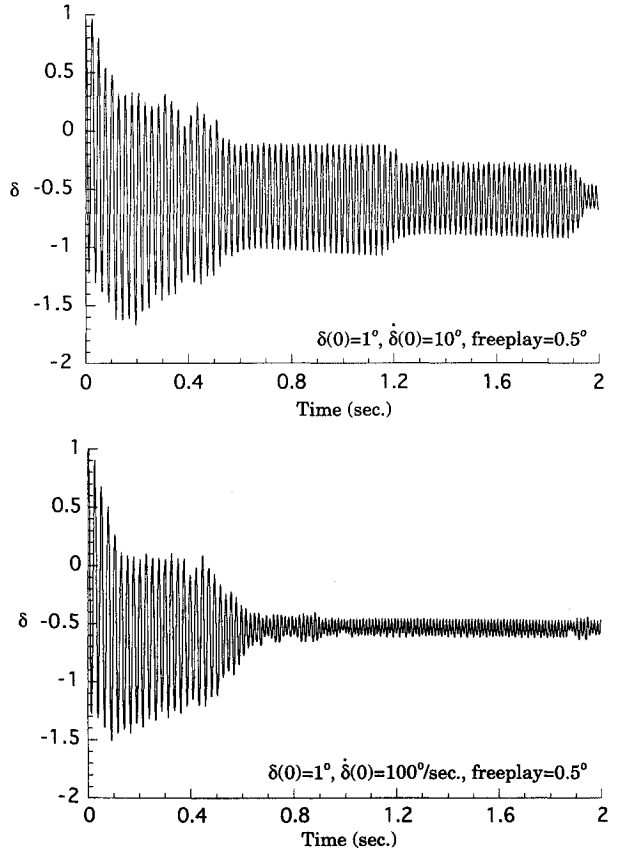

Fig. 11 Time history of flaperon LCO at $M = 0.97$, $\alpha = 2$ deg, and $h = 5000$ ft with different initial conditions.

deflection. Figure 11 illustrates the predicted LCO with 0.5 deg of freeplay, at nonzero initial deflections and velocities. It is found that the initial oscillation is developed in a similar fashion before $t = 0.5$ s, and then the one started with a higher initial velocity is quickly reduced to one with much smaller amplitude. The one with a lower initial velocity approaches a smaller amplitude in a slower manner. Again, these examples illustrate different phenomena attainable from different positions in the phase plane in a nonlinear system.

Conclusions

Forced oscillation testing of a flaperon on a rigid half-model of a fighter configuration was conducted to determine the properties of transonic limit-cycle oscillations. Instability was predicted by a clockwise hysteresis loop in the hinge moment response to flap deflection angle. Two flow control devices (i.e., the vortex generators and spoilers) have also been tested to eliminate the instability. Only the spoilers were found to be effective. The test technique allowed one to determine the best location and size of these spoilers. Test results were analyzed through Fourier functional analysis to establish a general forcing function for the control surface hinge moment. The forcing function was expressed in the form of nonlinear indicial integrals and could be used at frequencies other than the test frequencies. By integrating the structural equation of motion describing the control surface motion, simulation of control surface LCO time history was carried out by using Hamming's predictor–corrector method. The results of time history simulation indicated buzz might occur at $M = 0.97$ with the existence of structural freeplay. Because of mathematical nonlinearity, the initial conditions to induce limit-cycle oscillations were not obvious. A sure way to predict the possibility of control surface buzz was to examine the wind-tunnel data of forced oscillation at different frequencies. A triple loop in the plot of hinge moment coefficient vs deflection angle would indicate the existence of limit-cycle oscillation.

References

[1]Lambourne, N. C., "Flutter in One Degree of Freedom," *NATO AGARD Manual on Aeroelasticity*, Vol. 5, Feb. 1968, Chap. 5.

[2]Brown, H. H., Rathert, G. A., Jr., and Clousing, L. A., "Flight-Test Measurements of Aileron Control-Surface Behavior at Supercritical Mach Numbers," NACA RM A7A15, April 1947.

[3]Cunningham, A. M., Jr., "Practical Problems: Airplanes," *Unsteady Transonic Aerodynamics*, edited by D. Nixon, Vol. 120, Progress in Astronautics and Aeronautics, AIAA, Washington, DC, 1989, Chap. 3.

[4]Erickson, A. L., and Mannes, R. L., "Wind-Tunnel Investigation of Transonic Aileron Flutter," NACA RM A9B28, June 1949.

[5]Chin, S., and Lan, C. E., "Fourier Functional Analysis for Unsteady Aerodynamic Modeling," *AIAA Journal*, Vol. 30, No. 9, 1991, pp. 2259–2266.

[6]Hu, C. C., and Lan, C. E., "Unsteady Aerodynamic Models for Maneuvering Aircraft," AIAA Paper 93-3626, Aug. 1993.

[7]Bisplinghoff, R. L., Ashley, H., and Halfman, R. L., *Aeroelasticity*, Addison–Wesley, Cambridge, MA, 1955, Chaps. 5 and 6.

[8]Gerald, C. F., and Wheatley, P. O., *Applied Numerical Analysis*, Addison–Wesley, Reading, MA, 1984.

[9]Erickson, A. L., and Robinson, R. C., "Some Preliminary Results in the Determination of Aerodynamic Derivatives of Control Surfaces in the Transonic Speed Range by Means of a Flush-Type Electrical Pressure Cell," NACA RM A8H03, Oct. 1948.

[10]Herr, R. W., Gibson, F. W., and Osborne, R. S., "Some Effects of Flow Spoilers and Aerodynamic Balance on the Oscillating Hinge Moments for a Swept Fin-Rudder Combination in a Transonic Wind Tunnel," NACA RM L58C28, May 1958.

[11]Fuglsang, D. F., Brase, L. O., and Agrawal, S., "A Numerical Study of Control Surface Buzz Using Computational Fluid Dynamic Methods," AIAA Paper 92-2654, June 1992.

[12]Woolston, D. S., Runyan, H. L., and Andrews, R. E., "An Investigation of Effects of Certain Types of Structural Nonlinearities on Wing and Control Surface Flutter," *Journal of the Aeronautical Sciences*, Vol. 24, No. 1, 1957, pp. 57–63.